Disponible en **www.hormigonyacero.com**
https://doi.org/10.33586/hya.2025.4089

The Impact of Steel Fiber Length and Dosage on Microstructure and Mechanical Performance in UHPFRC: A Hybrid Approach

El impacto de la longitud y la dosificación de la fibra de acero en la microestructura y el rendimiento mecánico en UHPFRC: un enfoque híbrido

J.D. Ruiz Martínez[a], J.D. Ríos[b], E.M. Pérez-Soriano[c], H. Cifuentes[b], C. Leiva[a,*]

[a] *Department of Chemical and Environmental Engineering, Escuela Técnica Superior de Ingeniería, Universidad de Sevilla.*
[b] *Department of Continuum Mechanics and Structural Analysis, Escuela Técnica Superior de Ingeniería, Universidad de Sevilla.*
[c] *Department of Materials Science and Engineering and Transport, Escuela Politécnica Superior, Universidad de Sevilla.*

Recibido el 11 de febrero de 2025; revisado el 6 de mayo de 2025, aceptado el 26 de mayo de 2025

ABSTRACT

This study evaluates the effects of steel fiber length (6 and 13 mm) and dosage on the microstructural and mechanical properties of an ultra-high-performance fiber-reinforced concrete (UHPFRC). The incorporation of 6 mm fiber significantly improved the material's workability characteristics. Microscopic evidence indicates better alignment and distribution of 13 mm fibers within the concrete matrix compared to 6 mm fibers, resulting in reduced porosity and enhanced matrix-fiber interaction. Mechanical testing confirmed that the inclusion of 13 mm steel fibers at various dosages consistently outperformed 6 mm fibers in enhancing compressive and flexural strengths. The optimal dosage, among those tested, for compressive strength was found to be 196 kg/m³ with 13 mm fibers, while the best performance in flexural strength was observed at 226 kg/m³. To address the challenges inherent in UHPFRC—specifically the intricate metallic fiber distribution and limited workability prompted a comprehensive investigation into fiber mixture optimization strategies. Hybrid fiber approach was explored by substituting 10%, 20%, and 30% of the 13 mm fiber dosage (196 kg/m³) with 6 mm steel fibers. Among these, the mix containing 80% of 13 mm steel fibers and 20% of 6 mm steel fibers demonstrated the highest flexural strength, even than those with higher steel fiber content (226 kg/m³). This hybridization suggests an optimized combination of fiber lengths for enhanced flexural performance without compromising compressive strength, providing insights into effective fiber-reinforcement strategies for UHPFRC applications.

KEYWORDS: Ultra-high-performance concrete; steel fiber-reinforced concrete; fiber length; fiber hybridization; fiber-matrix interaction.

RESUMEN

Este estudio evalúa los efectos de la longitud (6 y 13 mm) y la dosificación de fibras de acero sobre las propiedades microestructurales y mecánicas de un hormigón reforzado con fibras de ultra altas prestaciones (UHPFRC). La incorporación de fibras de 6 mm mejoró significativamente la trabajabilidad del material. La evidencia microscópica indica una mejor alineación y distribución de las fibras de 13 mm dentro de la matriz del hormigón en comparación con las fibras de 6 mm, lo que se traduce en una menor porosidad y una interacción matriz-fibra más eficaz. Los ensayos mecánicos confirmaron que la inclusión de fibras de acero de 13 mm, en distintas dosificaciones, superó consistentemente a las de 6 mm en términos de resistencia a compresión y a flexión. La dosificación óptima para la resistencia a compresión fue de 196 kg/m³ con fibras de 13 mm, mientras que el mejor comportamiento en flexión se obtuvo con 226 kg/m³. Para abordar los desafíos de colocación característicos del UHPFRC —en particular la compleja distribución de fibras metálicas y la limitada trabajabilidad— se llevó a cabo una investigación exhaustiva sobre estrategias de optimización de mezclas con fibras. Se exploró un enfoque híbrido mediante la sustitución del 10%, 20% y 30% de la dosificación de fibras de 13 mm (196 kg/m³) por fibras de acero de 6 mm. Entre estas, la mezcla con un 80% de fibras de 13 mm y un 20% de fibras de 6 mm mostró la mayor resistencia a flexión, incluso superior a la de mezclas con mayor contenido total de fibra (226 kg/m³). Esta hibridación sugiere una combinación optimizada de longitudes de fibras para mejorar el comportamiento a flexión sin comprometer la resistencia a compresión, ofreciendo así nuevas perspectivas para el diseño eficiente de UHPFRC.

PALABRAS CLAVE: Hormigón de ultra altas prestaciones, hormigón reforzado con fibras metálicas, longitud de la fibra, hibridación de fibras, interacción matriz-fibra.

* Persona de contacto / *Corresponding author*:
Correo-e / *e-mail*: cleiva@us.es (Carlos Leiva Fernández)

Cómo citar este artículo: Ruiz, J.D., Ríos, J.D., Pérez, E.M., Cifuentes, H., & Leiva, C. (2025). The Impact of Steel Fiber Length and Dosage on Microstructure and Mechanical Performance in UHPFRC: A Hybrid Approach.. *Hormigón y Acero*. 76(306):65-76. https://doi.org/10.33586/hya.2025.4089

1. INTRODUCTION

Over the past 20 years, ultra-high performance concrete (UHPC) has gained popularity for its exceptional mechanical properties, even competing with structural steel [1,2]. UHPC boasts a minimum compressive strength of 130 MPa and a flexural tensile strength over 12 MPa, with a notable opportunity for improvement in ductility [3,4]. Because of its nearly complete porosity, it is extremely resistant to aggressive and acidic substances penetrating into its matrix [5–7]. UHPC usually offers more than three times the compressive strength and approximately six times the flexural tensile strength of ordinary concrete, enhancing its ductility and energy absorption capacity [8]. It has also been widely employed in pavements, airport runways, and long-span bridge decks, which require excellent performance under flexural strain [9]. The use of UHPC allows for the reduction in the size of structural components and, consequently, the overall weight of the structure. This reduction leads to lower labor, maintenance, and shipping expenses, contributing to sustainability [10]. UHPC manufacturing presents substantial processing challenges, primarily attributed to its restricted water-to-binder proportion, intricate macro metallic fiber distribution, and markedly diminished workability [11,12].

The steel fibers are used for improved structural performance, typically employed for UHPC at a content of 2% to 3% by volume. According to Skazlić and Bjegovic [13], when the fiber volume content is 3%, the flexural behavior of Ultra High Performance Fiber Reinforced Concrete (UHPFRC) deteriorates with the use of long steel fibers due to poor fiber dispersion and fiber balling. Steel fibers with dimensions of 13 mm in length and 0.20 mm in diameter are the most widely utilized sizes [14]. As a result, is a composite material in which the inclusion of fibers improves the mix's characteristics, particularly its tensile and fracture qualities, but also has the potential to create voids and encourage the initiation and development of microcracks within the matrix [15–19]. In UHPFRC, the effectiveness of the fiber in improving mechanical properties, such as strength and ductility, through effective stress transfer and crack bridging mechanisms is typically only 30% and fiber orientation is erratic [20]. Experimental results affirmed that better fiber alignment correlates with increased flexural strength and toughness in UHPFRC [21]. Minimizing the fiber reinforcement volume without sacrificing its performance is crucial since UHPFRC places a strong emphasis on sustainability and economic efficiency [22,23].

Hybridization of different steel fiber lengths to improve use efficiency and fiber quantity presents a promising opportunity for further development. It has been demonstrated that combination of short (13 mm) and medium length (19.5 mm) stainless steel fibers significantly improves the flexural performance of UHPFRC [24]. Yoo et al. [25] found that hybrid of long and medium-length fibers improves flexural performance of UHPFRC. The length of the fibers is a critical factor: shorter fibers may not bond effectively with the matrix, potentially leading to slippage and reduced crack resistance, whereas longer fibers increase the contact area and strengthen the bond [26]. Outcomes in line with Rios et al. [18] found that the hybrid reinforced mix of steel fibers produced better fracture behavior because the presence of straight fibers (13 mm) increased the matrix's cracking strength and caused larger deformations prior to the hooked end fibers (30 mm) debonding.

The aim of this work is to study the influence and effectiveness of straight steel fibers of different lengths (some are under explored as 6 mm) on the flexural and compressive properties of UHPFRCs. Complementarily, the workability of fresh concrete, key factor for the on-site application of this type of concrete, as well as the porosity of the compositions were investigated to establish a correlation with their mechanical properties. Evidence was also extracted with a stereomicroscope of the dispersion and orientation of the fibers when casting fresh concrete. Based on comprehensive experimental results and with the objective of enhancing workability without compromising mechanical performance, the best dosage of hybridization to reinforce the UHPFRC was established.

2. MATERIALS AND SPECIMEN PREPARATION

2.1. Materials

For the cementitious matrix, a mix of three binders were used in this study. Type I cement 52.5 R/SR (Portland Valderrivas, Spain) complies with EN 197-1:2011 [27]. The ground-granulated blast-furnace slag (GGBS) provided by Arcelor-Mittal, and the silica fume (SF) S-92-D provided by SIKA. Two varieties of quartz sand were used as aggregates: the finest sand (FS) had a maximum particle size of 0.315 mm, while the coarse aggregate (CS) had particles less than 0.800 mm [12]. Bekaert provided two type of the steel fibers, which were 6 and 13 mm in length (designated as F6 and F13) and 0.15 mm and 0.2 mm in diameter respectively (Table 1). Sika supplied the superplasticizer (20HE).

2.2. Mix proportions and sample preparation

Initially twelve different mixes of UHPFRC that differed only in steel fiber type and content were manufactured. Ta-

TABLE 1.
Properties of Steel Fiber

Fiber	Diameter (d_f) (mm)	Length (l_f) (mm)	Aspect ratio (l_f/d_f)	Density (g/cm³)	Tensile strength (MPa)	Elastic Modulus (GPa)
F6	0.15	6	6/0.15 = 40	7.8	2500	200
F13	0.2	13	13/0.2 = 65	7.8	2500	200

ble 2 shows the designation of the mixes and the proportion of constituents of each.

The manufacturing process of these types of concretes plays a crucial role in the final properties of the matrix, which is why it is detailed below. The solid materials – cement, SF, GGBS, FS and CS – were mixed for 5 minutes in a vertical mixer to achieve a homogeneous solid mix. Subsequently, the super-plasticizer and water were added and mixed for 20 minutes to achieve a workable consistency. Finally, steel fibers were added and mixed for five more minutes. For each of the mixes, three 40x40x160 mm³ prisms were cast. After 24 hours, the samples were demolded and subjected to a further curing period of 26 days submerged in water at room temperature. Finally, the samples were left to dry for 48 hours. The selected fiber volume fractions ranged from 2.24% to 2.88%, consistent with values reported in the literature for structural-grade ultra-high-performance fiber-reinforced concrete (UHPFRC). This dosage range ensures sufficient performance for structural applications while promoting uniform fiber dispersion and mitigating workability issues such as fiber balling or excessive mix stiffness–challenges typically encountered at higher fiber contents. Given that UHPFRC must inherently exhibit self-compacting behavior, maintaining this range is critical. Furthermore, over the past decade, our research group has conducted extensive investigations on fiber-reinforced UHPC, consistently achieving optimal mechanical performance within this dosage interval. [28,29]

2.2.1. Hybrid Mix proportions and sample preparation

The proposal has been based on the dosage of 196 kg/m³ of 13 mm fiber for its better performance in porosimetry and consequently compressive strength. Concerted percentages are replaced by 6 mm fibers to measure the effectiveness of hybridization. This decision balances performance and resource efficiency by avoiding the higher fiber dosage that, even though it offers improvements in flexural performance, presents problems related to fiber dispersion and possible bunching of the fiber that compromises compressive performance. Therefore, the 13 mm fiber mix with 196 kg/m³ was replaced by 10%, 20% and 30% with 6 mm fiber content, in order to observe its mechanical behavior.

3. EXPERIMENTAL PROGRAM

3.1. Workability

To assess the workability of fresh concrete, a downscaled slump test was developed in accordance with the guidelines provided in EN 12350-2:2020 [30] standard. A modified Abrams cone geometry with dimensions of 50 mm at the top, 100 mm at the bottom, and 150 mm in height was used as the setup for the mini-slump test in this work. The reduced

TABLE 2.
Mix proportions and designation.

	Constituent (kg/m³)								
Mix	**Cement**	**SF**	**GGBS**	**FS**	**CS**	**Water**	**SP**	**6 mm Steel fibers**	**13 mm Steel fibers**
F6_176	540	210	310	470	470	205	42	176	
F6_186								186	
F6_196								196	
F6_206								206	
F6_216								216	
F6_226								226	
F13_176									176
F13_186									186
F13_196									196
F13_206									206
F13_216									216
F13_226									226

TABLE 3.
Mix proportions and designation of fiber hybridization.

	Constituent (kg/m³)								
Mix (196 kg/m³)	**Cement**	**SF**	**GGBS**	**FS**	**CS**	**Water**	**SP**	**6 mm Steel fibers**	**13 mm Steel fibers**
F90/10								19.6	176.4
F80/20								39.2	156.8
F70/30								58.8	137.2

cone used has dimensions that are half those of the standard Abrams cone, resulting in approximately half the volume of concrete. Based on this, and following previous literature [31], a mini slump flow value of 275 mm was considered equivalent to the 550 mm limit used in the conventional slump flow test to classify a mixture as self-compacting.

3.2. Steel Fiber Dispersion and orientation

For the study of the dispersion and orientation of the fibers, slices of the prismatic molds were obtained by saw cutting. A cross-section measuring 20 × 20 mm² was obtained from the center of each prism of 40 x 40 mm², This central position was chosen to minimize boundary effects and ensure a representative measurement of fiber distribution.. Based on previous literature [32] who have used ellipse-based image analysis techniques to quantify orientation with higher precision, our approach relies on optical microscopy and visual examination to assess horizontal alignment trends in fiber distribution. The samples were subsequently roughened, finely ground, and polished to achieve a smooth surface for analysis. A Nikon Microscope eclipse (MA100N, New York, USA), coupled with a PC running NIS-Elements BR image capture software, was utilized. This setup enabled detailed microscopic observations of the fiber alignment and their interactions with the cementitious matrix [33,34].

3.3. Porosity

A Micromeritics Autopore IV mercury intrusion porosimeter (Norcross, USA) was used to measure porosity. Pore sizes varied between 150 µm and 0.007 µm. The 5 mm pellets were obtained from the tested samples and drying them in an oven at 105 °C to remove moisture.

3.4. Mechanical properties

3.4.1. Compressive strength

For each type of mix, six 80x40x40 mm³ samples were tested to evaluate compressive strength in compliance with EN 12390-3 [35]. This test was conducted using a servo-hydraulic testing apparatus with a 3000 kN load capability.

3.4.2. Flexural strength

Three-point bending tests were performed on each of the concrete designs used in this study. The tests were carried out in compliance with EN 14651[36]. The specimens prepared for these testing have the following dimensions: 40x40x160 mm³. A central notch was made in each specimen to a depth equal to one-sixth of its height. A 5-mm clip-on displacement gage was used to measure the crack mouth opening displacement (CMOD) during the test, and a 10-mm vertical transducer was used to record the deflection at the specimen's center. Servo hydraulic bending testing machine with CMOD displacement control that can resist a maximum load of 200 kN was used for the studies, The f_L value was identified as the maximum flexural strength within the 0.05 mm CMOD range, as defined by EN 14651 [36]. The f_L value, which represents the cracking strength, triggered tensile cracking in the UHPFRC beam, also referred to as Limit of Proportionality (LOP).

The residual strength is determined using equation (1), and the tests and outcomes were carried out in accordance with EN 14651 standard [36]:

$$f_{Rj} = \frac{3P_jL}{2bh_{sp}^2} \quad (1)$$

where f_{Rj} and P_j, which correlate to $CMOD_j$, stand for the applied load and residual flexural tensile strength, respectively. More specifically, the corresponding CMOD values of 0.5 mm, 1.5 mm, 2.5 mm, and 3.5 mm were used to determine f_{R1}, f_{R2}, f_{R3}, and f_{R4}. Equation (1) uses b for the beam's width, hsp for the beam's height (not including the notch height), and L for the span length.

4. RESULTS

4.1. Workability

The workability test was conducted on mixes with varying dosages (176, 196, 226 kg/m³) of two different lengths of steel fibers. The results indicated a clear trend: as the steel fiber content increased, the slump diameter decreased. Additionally, the results demonstrated that larger fibers resulted in lower workability for the same content. The results of the slump tests for each mix are depicted in Figure 1.

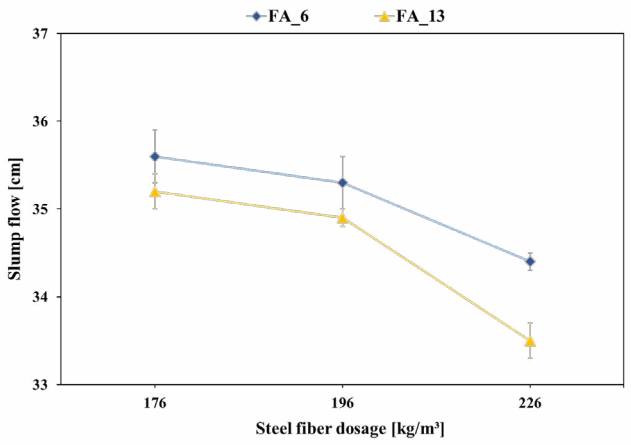

Figure 1. Mini slump flow images for representative mixes.

As shown in Figure 1, mixes with shorter fiber lengths exhibit larger slumps diameters, suggesting less fiber entanglement due to the shorter fibers. Furthermore, as illustrated in Figure 2, all mixes demonstrated self-compacting characteristics, achieving a diameter slump greater than 30 cm without deformation or segregation. This indicates that even with substantial reinforcement, the UHPFRC can flow and fill formwork under its own weight without the need for vibration, maintaining a consistent consistency throughout [37].

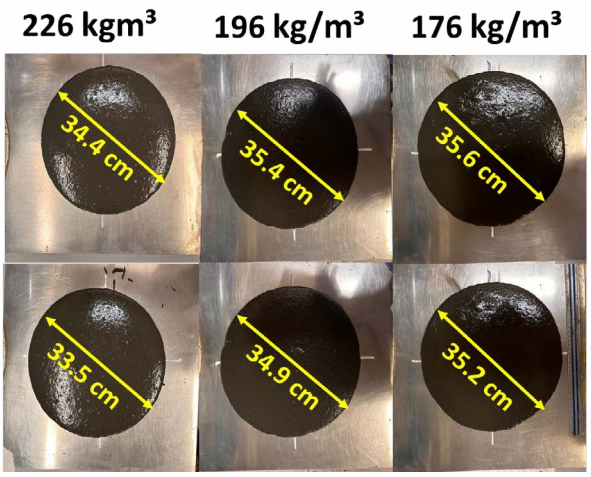

Figure 2. Mini slump flow measurements were conducted on UHPFRC samples containing varying steel fiber dosages and lengths.

4.2. Steel Fiber Dispersion and Orientation

Figure 3 shows images of the interaction between the steel fibers and the cementitious matrix after the curing process obtained from the cut samples. A microscopic approximation of the specially fabricated samples is made, with the focus on the orientation and dispersion of the fiber as the concrete is cast.

Previous research states that there is a positive correlation between the orientation and the UHPFRC's tensile characteristics. In steel fiber reinforced UHPC, the orientation of the fiber should be perpendicular to the fracture orientation, this allows steel fibers to efficiently bridge the crack and support the load [14,18,38,39].

The Figure 3 comparison reveals that, with the same dosage of steel fibers, the shorter fibers (6 mm) are more frequently observed due to their greater quantity (F13:118 – F6:136) compared to the longer fibers (13 mm). However, the 6 mm fibers appear to be less horizontally aligned, in the direction perpendicular to, with a noticeable increase in vertically oriented fibers. Additionally, the distribution of the 6 mm fibers seems inadequate, as certain areas lack any visible fibers, indicating a non-uniform dispersion within the matrix.

The longer fibers, due to their larger contact surface, and therefore higher surface tension, tend to settle more easily into a horizontal position under the influence of gravity. In contrast, the shorter 6 mm fibers, lighter and smaller, can remain more randomly oriented, often vertical.

Figure 4 compares the steel fibers of 13 mm length at dosages of 196 kg/m³ and 226 kg/m³. As expected, the figure corresponding to 226 kg/m³ exhibits a higher density of fiber points (F13_226:153 – F13_196:118). However, it also shows poorer longitudinal alignment of fibers (perpendicu-

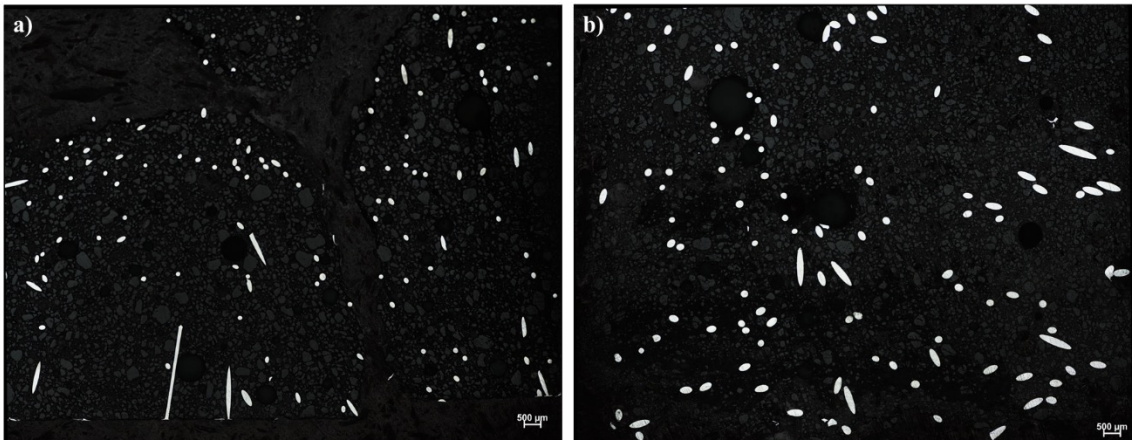

Figure 3. Comparison of Steel Fiber Orientation and Dispersion of a) F6_196 and b) F13_196.

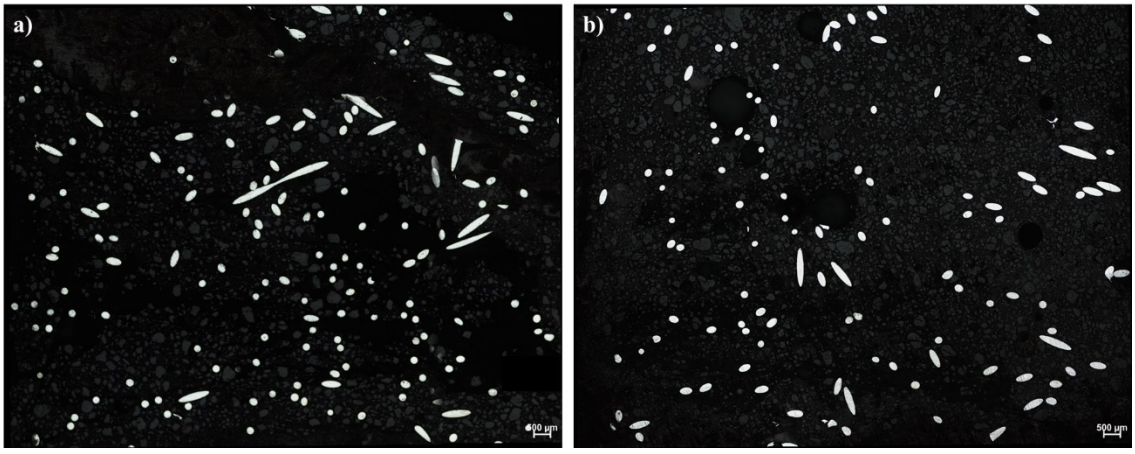

Figure 4. Comparative Image of steel fiber orientation and dispersion of a) F13_226 and b) F13_196.

lar to the bending stress), which, as previously mentioned, reduces their efficiency. Furthermore, the reduction in workability, as illustrated in Figures 1 and 2, is linked to the impaired orientation and dispersion of the steel fibers.

4.3. Porosity

Porosity is a crucial factor in determining the mechanical properties of concrete. Increased porosity in a concrete matrix reduces the solid surface contact area between particles [40]. As shown in Figure 5 and table 4, there are three different pore ranges: capillary pores (less than 0.1 µm in diameter), micropores (0.1–10 µm in diameter), and macropores (greater than 10 µm in diameter). The three main parameters in the pore distribution are: 1) the pore size, 2) pore volume, and 3) Steel Fiber dosage.

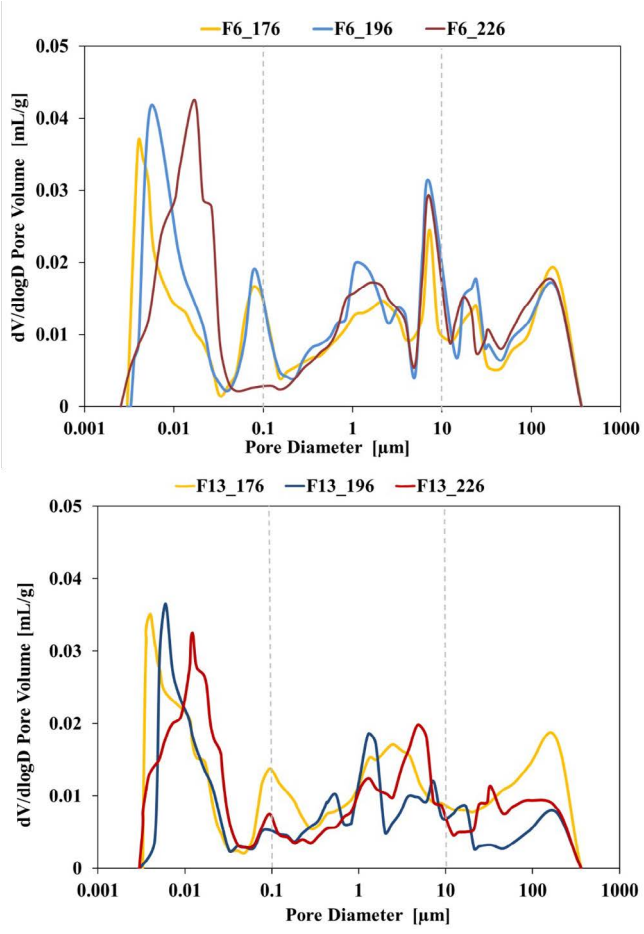

Figure 5. Pore size distribution of representative mix containing 6mm and 13mm steel fiber.

The porosimetry results in Figure 5 and Table 4 reveals the pore distribution across the different UHPFRC mixes. Figure 5 shows that most of the pores are capillary pores in all dosages, especially in the 6 mm composites. F6_176 has a higher amount of macropores compared to other quantities of steel fibers in both lengths. Ríos et al. [18,19] demonstrated by X-ray tomography that micro pores and voids are mostly concentrated around the steel fibers, because the fibers act as blades that divide the macropores into micropores and capillary pores, so it would be logical that the higher the amount of fiber, the higher the capillary pores. However, the 226 kg/m³ mix shows a slightly larger quantity of micropores than 196 kg/m³, probably due to bunching or excess fiber distribution (Figure 4).

TABLE 4.
Pore volume of representative mix containing 6mm and 13mm steel fiber.

	Pore Volume (mL/g)		
Mix	**<100 nm**	**100–10000 nm**	**>10000 nm**
F6_176	0.233	0.214	0.122
F6_196	0.269	0.246	0.106
F6_226	0.297	0.225	0.117
F13_176	0.163	0.223	0.096
F13_196	0.187	0.202	0.053
F13_226	0.195	0.193	0.060

Regarding capillary pores, the addition of more steel fibers increases the pore volume by 27.3% for F6, while for F13 it increases pore volume by 19.4%. While talking about macro porosity, the effect experienced is adverse, reducing the pore volume by –12.7% for F6 and –37.4% for F13 in the dosages with the lowest macro porosity (196 kg/m³). This could be explained by the effect of the fiber in dividing the large pores into micro and capillary pores.

4.4. Mechanical and fracture properties

4.4.1. Compressive strength

Figure 6 compares the effect of different dosages and fiber lengths on the compressive strength of UHPFRC. The 6 mm fibers exhibit a consistent upward trend in compressive strength as fiber dosage increases. The best performance was shown by the dosage of 216 kg/m³, the compressive strength peaks at 151 MPa. Overall, an increase of 14% is observed compared to the initial dosage. However, the highest dosage (226 kg/m³) shows an adverse trend by dropping to 135 MPa (-10.2%), due to a fiber saturation that does not allow the fibers to take the horizontal position to develop their mechanical function, as shown in Figure 3a.

For the 13 mm fibers, the results do not follow a clear upward trend. The best result is obtained at 196 kg/m³, where the strength reaches 161 MPa, marking an additional 12% increase compared to the lower dosage. However, beyond this point, a decline is noted. At 206 kg/m³, the strength drops back to 149 MPa and remains almost stable at 226 kg/m³ with 146 MPa. It is remarkable that compression mechanisms are clearly related to porosity (Figure 5), where the dosage with the lowest amount of macropores showed the best results in compression (196 kg/m³).

Across the range of dosages, 13 mm fibers generally outperform the 6 mm fibers. The maximum compressive strength for 13 mm fibers is 161 MPa, whereas the maximum for 6 mm fibers is 151 MPa. However, the 13 mm fibers peak earlier, at 196 kg/m³, while the 6 mm fibers show steady improvement up to 226 kg/m³.

On average, the 13 mm fibers show approximately 10% higher performance compared to the shorter fibers across most

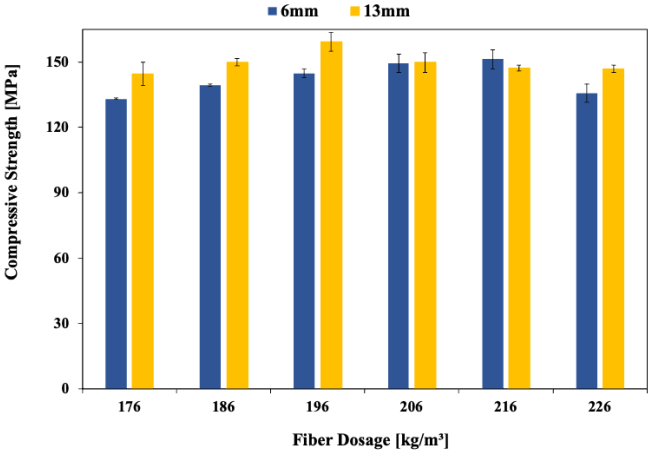

Figure 6. Compressive strength results of each mix.

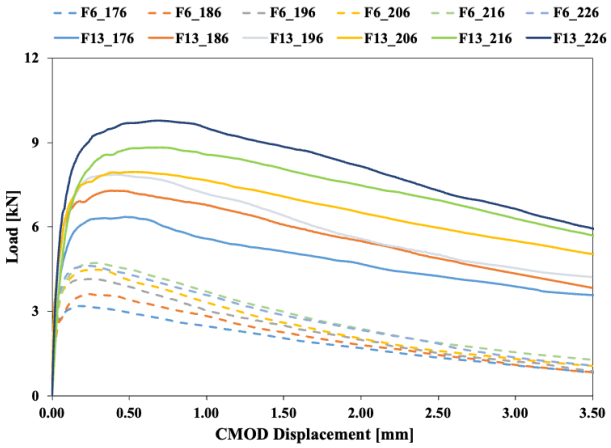

Figure 7. Average Load-CMOD curves for all mixes.

TABLE 5.
Limit of proportionality and residual strengths for each mix.

Mix	LOP, f_L (MPa)	f_{R1} (MPa)	f_{R2} (MPa)	f_{R3} (MPa)	f_{R4} (MPa)
F6_176	9.3	10.0	6.9	4.6	2.7
F6_186	9.8	12.1	8.2	5.5	3.4
F6_196	11.1	13.8	8.7	5.4	3.6
F6_206	11.6	14.9	8.7	5.4	3.6
F6_216	11.9	16.7	10.9	6.9	4.7
F6_226	11.6	14.5	9.6	6.2	3.6
F13_176	13.7	19.1	15.6	13.0	11.0
F13_186	15.9	23.8	19.9	16.2	13.5
F13_196	16.4	26.0	21.2	16.6	13.9
F13_206	17.3	27.8	22.9	19.1	16.0
F13_216	18.5	29.7	27.2	23.4	19.2
F13_226	19.4	32.7	29.8	24.6	20.1

dosages, except at the highest dosage of 216 kg/m³, where the 6 mm fibers slightly surpass the 13 mm fibers. This behavior suggests that while 13 mm fibers are more effective at lower dosages, 6 mm fibers offer a more reliable improvement in compressive strength as the fiber content increases, except for the highest dosage. This compressive strength behavior is in line with the porosimetry results (Table 4), especially linked to the macropore volume.

4.4.2. Evaluation of residual flexural strength and LOP

The experimental findings for the proportional limit and residual strengths derived from three-point bending tests are shown in Table 5 and Figure 7.

Fracture curve models are essential for calculating the propagation of cracks and have been used to describe both pre- and post-cracking behavior in concrete [41,42]. The references mentioned state that there are three distinct stages in the UHPFRC failure process. 1) Linear or elastic phase: the fibers and cement matrix cooperate to withstand applied loads during this first stage, reflected in the LOP. 2) Cracking zone or nonlinear phase: microcracks form during this phase. The growth of these microcracks is gradually resisted by the fibers incorporated into the matrix, behavior reflected in fR1. 3) Stable propagation phase, also known as the post-cracking zone, during which the load is supported by the fibers at the macrocrack surface, ultimately resulting in total fiber detachment, which is reflected in the different highly correlated values of fR2, fR3 and fR4. The behavior of fiber pull-out is mostly associated with the mechanical performance of the UHPFRC mixes in the post-cracking regime [43,44].

Figure 7 presents the Load–CMOD curves for all tested mixes, obtained from the three-point bending test. These curves provide a detailed representation of the flexural behavior, including peak load capacity and post-peak softening response. As observed, the incorporation of 13 mm fibers (solid lines) significantly improves both the maximum load-bearing capacity and the residual load-carrying ability after cracking, in comparison with the mixes containing 6 mm fibers (dashed lines). This graphical representation complements the tabulated data and may serve as a useful reference for the calibration and validation of numerical models.

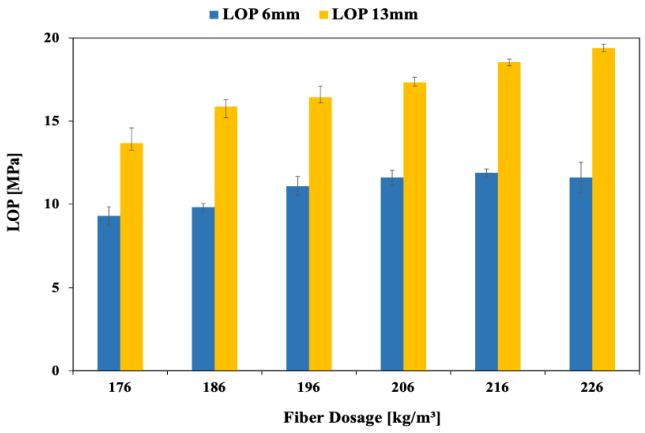

Figure 8. LOP values for the different dosages of 6 and 13 mm fibers.

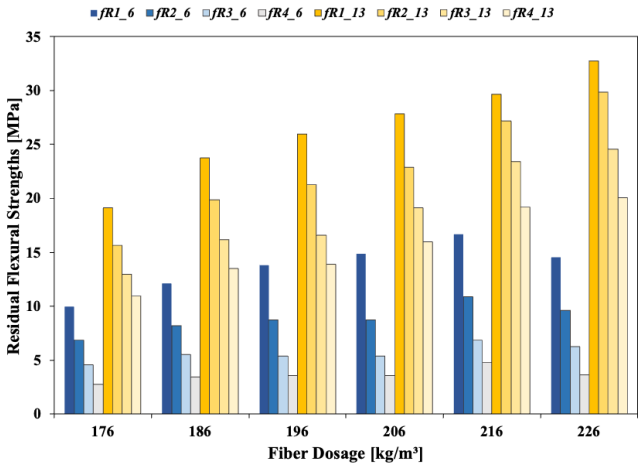

Figure 9. Residual strengths of each composition.

The data provided in Figure 8 shows the LOP values for the different dosages and lengths. It reveals a significant improvement within the efficiency of 13 mm fibers compared to the fibers with lengths of 6 mm, specifically within high dosages. The highest difference in the two strands is reflected at the dosage of 226 kg/m³, where the 13 mm stands at a strength of approximately 19.4 MPa. This is substantially much higher than that of 6 mm, which is 11.6 MPa. This underlines the improved capability of the extended fibers to increase the flexural properties of the material when used at higher dosages.

In the case of the 6 mm fibers, there is a gradual rise in the LOP values with the increase in fiber dosage. As in compressive strength (Figure 6), the peak performance occurs at 216 kg/m³ dosage, where the LOP is about 11.9 MPa. This reflects a gain of 15%, compared to the LOP value recorded at the lowest dosage of 176 kg/m³, which starts at approximately 9.3 MPa. Notwithstanding this enhancement, the 6 mm fibers exhibit a more conservative pattern in comparison to the 13 mm fibers, suggesting that the shorter fibers are less efficient in markedly elevating the material's proportionality limits when subjected to load.

In contrast, the 13 mm fibers exhibit clear linearity in growth with fiber dosage. Starting with a dosage of 176 kg/m³, where the LOP is 13.7 MPa, as the fiber dosage increases, reaching a peak of 19.4 MPa (+41%) at the highest dosage level of 226 kg/m³. This progressive improvement shows that higher percentages of these fibers directly benefit the LOP values by showing their capability to sustain higher relative stresses before yielding or the onset of cracking.

4.4.3. Influence of LOP on residual flexural strengths

A matrix with a high LOP corresponds to an improvement in initial linear-elastic properties and a higher residual strength of the concrete. This is because steel fibers act against the first instances of microcracking, forcing the cracks to follow much more complicated routes that are many times more energy-intensive. These fibers help in sustaining the integrity of the matrix due to the difficulty of crack propagation, hence giving higher residual strength even past attainment of the LOP in the matrix where microcracks have started to appear [45–47].

In this phase a strong relation occurs between LOP and residual strengths determined at f_{R1} (0.5 mm CMOD) and f_{R2} (1.5 mm CMOD). The residual strength curves exhibited sharp rises in the early stages within the region of lower values of CMOD which is indicative of the resistance of the matrix to cracking, enhanced by the fibers.

Nevertheless, when crack openings exceed 2.5 mm CMOD (f_{R3}), there is a noticeable reduction in the rate of increase of residual strength. This phenomenon occurs as the matrix's capacity to support loads diminishes progressively with the widening of the cracks, resulting in a redistribution of stress toward the fibers. At this juncture, the fibers assume a more prominent function in spanning the cracks and supporting the loads [19,48]. In fact, the transition of forces can be realized from the f_{R4} (3.5 mm CMOD) measurements, as the residual strength gain plateaus out after the previous stages. Thus, even though the matrix dominates the initial stages of crack development, the fibers dominate the later stages of crack growth and, hence, significantly control the further crack growth and enable an enhancement in residual strength in the composite material.

As can be seen in Figure 9, 13 mm fibers show higher performance than that of 6 mm with most significant gap between them at the highest fiber dosage of 226 kg/m³. In this dosage, f_1 and f_{R2} for the 13 mm fibers reach up to about 30 MPa, whereas for the 6 mm fibers, the residual strength is substantially lower, with a maximum residual strength value of around 16 MPa. This behavior of the longer fibers is correlated with the results reflected in Figure 3, where better horizontality and distribution of those longer fibers were seen within the UHPFRC matrix. This improved distribution enables the 13 mm fibers to bridge the macrocracks more effectively, allowing better stress transfer across the fibers [40,49].

Since these observations are related to the trends in LOP given in Figure 8, it is obvious to note that the 13 mm fibers showing improved LOP behavior also exhibit better residual strength behavior in the whole range of CMOD. With further crack propagation, the contribution of the matrix be-

comes small, and the fibers become the main load-carrying elements, primarily the longer 13 mm fibers. This explains why the residual strengths of the 13 mm fibers increase linearly with increasing dosage, whereas the 6 mm fibers reach a peak earlier (lower dosage).

It is also worth mentioning that on average, the percentage variation between the LOP of F6 and F13 is 55%, but this value increases in the residual forces, reaching an average of 95% in f_{R1} and reaching a percentage variation of 330% in f_{R4}. These findings provide critical insights into fiber performance mechanisms. Short fibers demonstrate effectiveness in mitigating microcracks and dissipating energy prior to initial crack formation. Conversely, long fibers exhibit superior performance throughout the entire testing process, with exceptional capabilities in resisting macro-crack propagation.

5. FIBER HYBRIDIZATION APPROACH

Based on the obtained results and previous research, proven the ability of small fibers to delay fracture initiation while long fibers are able to reduce fracture propagation, hybrid composites were prepared with fibers of different lengths to further improve their performance and effectiveness.

This series of research focuses on hybridizing fibers of different lengths for their microstructural implications and its consequence on the flexural and compressive properties, with a view to optimizing the strength of both fiber types in seeking an optimal balance between workability, crack mitigation, and load-bearing capacity.

The workability of hybrid compositions, as shown in Figure 10, follows the expected trend. As the proportion of shorter fibers within the 196 kg/m³ dosage increases, a slight improvement in workability is observed. This is consistent with the behavior observed in the previous test, where smaller fibers contributed to a smoother mix. By increasing the percentage of shorter fibers, the matrix flows more easily, facilitating better fiber dispersion and improving overall workability. This is important as it represents an advantage in the civil implementation [6].

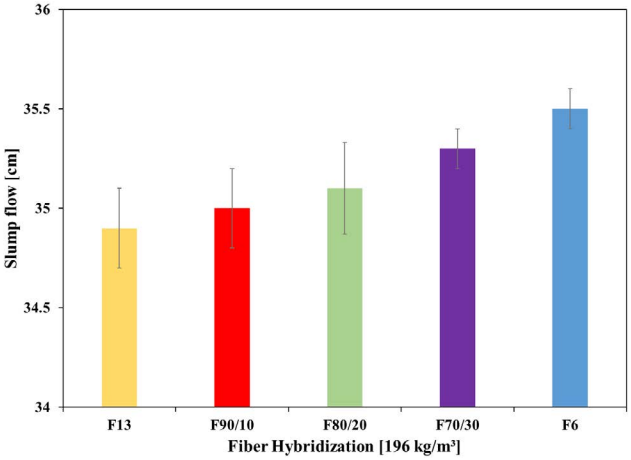

Figure 10. Mini slump flow diameter for hybridization mixes.

Figure 11 illustrates the distribution and orientation of fibers in the hybridization configuration 80/20, which subsequently demonstrated better performance, compared to image containing only 13 mm fibers (Figure 4b).

It is evident that in hybridization, the shorter fibers (smaller white circles) are properly integrated with the longer fibers (larger white circles) and are more evenly distributed within the matrix. In addition, the horizontal alignment of the fibers, which can be seen in the circularity of the white dots, indicates a more efficient working of the fiber flexural stresses, and is noticeably better in the hybrid configuration (Figure 11) than in the F13_226 mix (Figure 4a), even better than in the F13_196 mix (Figure 4b).

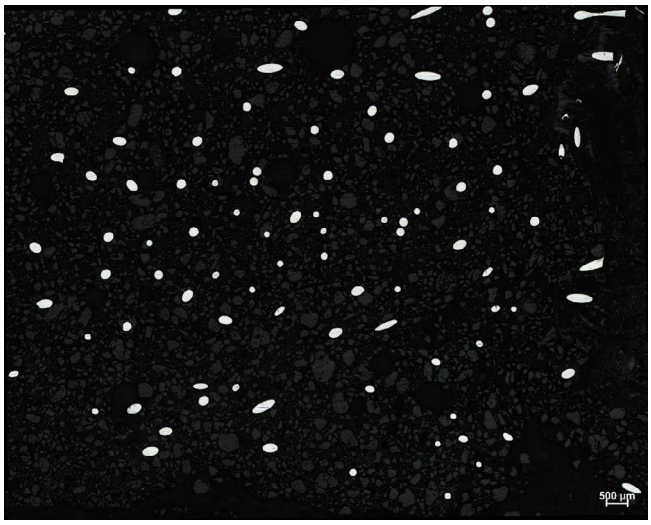

Figure 11. Image of Steel Fiber Orientation and Dispersion of F80/20_196 Mix.

Figure 12 illustrates the porosity of different proportions of fiber hybridization with varying fiber lengths. As seen in Table 6, in terms of porosity, no significant improvement has been achieved compared to the reference dosage of 13 mm.

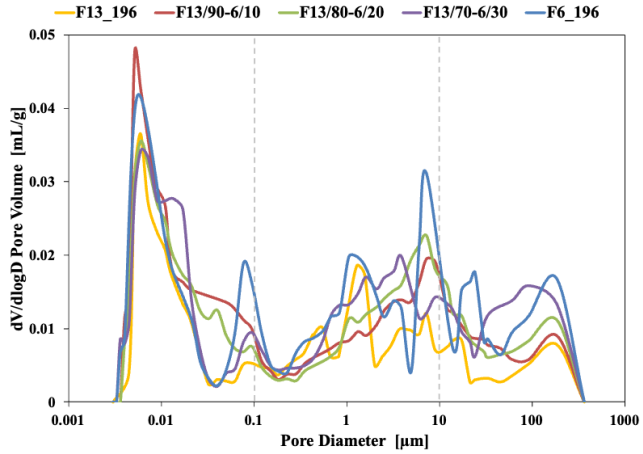

Figure 12. Porosimetry analysis for hybridization mixes.

The results indicate that the amount of macropores (with diameters larger than 100 µm) is higher in all hybrid mixes

compared to the reference, but as expected, they improve the macroporosity of the 6 mm fiber composition, with the 90/10 composition showing the best performance among the three hybrid mixes regarding total porosity. In terms of micropore distribution (diameters less than 0.1 µm), the 90/10 and 13 mm mix outperform as a consequence of the large pores divided into small pores. Among the other compositions, there are no evident differences.

TABLE 6.
Pore volume of hybrid and reference mix (196 kg/m³).

	Pore Volume (mL/g)		
Mix	<100 nm	100–10000 nm	>10000 nm
F6_196	0.269	0.246	0.106
F_70/30	0.312	0.222	0.104
F_80/20	0.316	0.220	0.102
F_90/10	0.321	0.201	0.097
F13_196	0.187	0.202	0.053

Figure 13 presents the compressive strength results for different hybrid fiber compositions, with a 196 kg/m³ dosage. The three hybrid mixes displayed very similar results to each other, maintaining comparable compressive strengths slightly below the reference but still higher than the mix containing only 6 mm fibers.

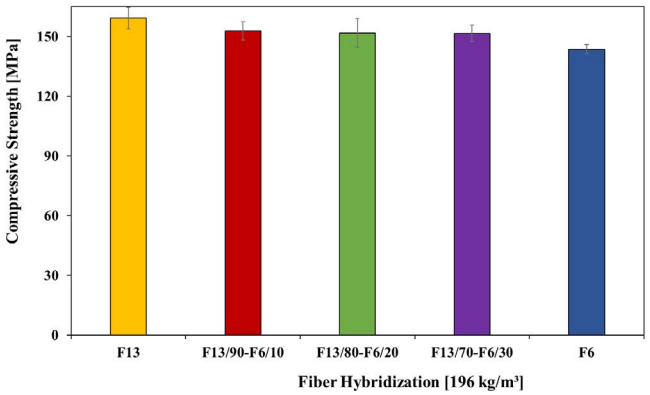

Figure 13. Compressive Strength for hybridization mixes.

The consistency in the results across the hybrid mixes can be linked to the macroporosity findings. As discussed previously (Figure 11), the F13 mix showed fewer macropores, explaining its superior compressive strength. The hybrids, while not reducing macroporosity as effectively, still managed to significantly improve compressive behavior compared to the F6 mix, which had the lowest performance in both porosity and strength. This indicates that the combination of fiber lengths achieves a balance, where microstructural improvements such as reduced macropore formation may not be fully realized, but the hybrid fibers still contribute positively to maintaining compression strength.

Figure 14 presents the LOP and residual flexural strength (f_R) for different hybrid fiber compositions at a dosage of 196 kg/m³. When comparing these hybridized mixes to the reference mix containing only 13 mm fibers (F13), it is evident that all hybridizations improve flexural performance. Specifically, the F 90/10 mix shows a modest 4% increase in strength, while the 80/20 hybridization achieves a more substantial 25% improvement in LOP. This proves that incorporating a controlled ratio of shorter fibers enhances the ductility of the matrix more effectively than using only one length steel fibers.

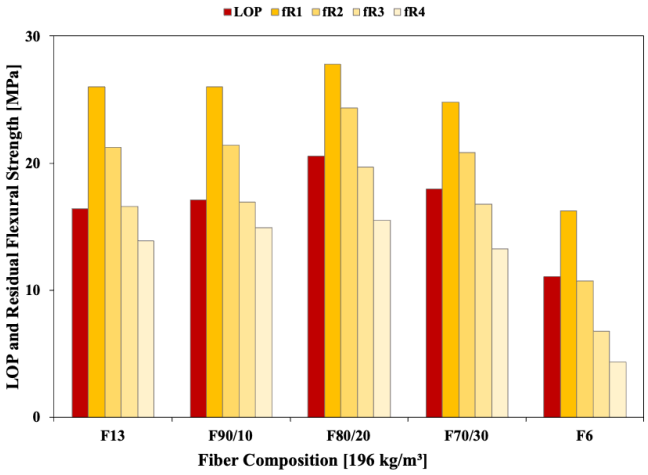

Figure 14. Limit of Proportionality (LOP) and Residual Flexural Strength (fR) for different hybrid fiber compositions at a dosage of 196 kg/m³.

Notably, the highest peak in LOP is achieved by the 80/20 hybrid mix, reaching 20.5 MPa, which even surpasses the performance of a higher fiber dosage of 226 kg/m³ that had a LOP of 19.4 MPa. This exceptional result highlights the efficiency of the 80/20 composition in optimizing initial flexural strength, making it the most effective among the tested mixes. This results in a more even fiber distribution and greater alignment of the fibers along the longitudinal plane (perpendicular to the bending stress) (as seen in Figure 12).

The behavior of the residual flexural strength (f_{R1} to f_{R4}) also reveals important insights. As the proportion of shorter fibers decreases, the gap between the LOP and the residual strengths becomes bigger, (86% for F90/10 against 74% for 70/30 between f_{R1}-f_{R4}) indicating that while the hybridization improves the elastic performance, its impact on residual strengths capacity is less effective. Explained because the presence of short fibers enhances the matrix's performance, increasing the toughening effect of the fibers on the matrix, thereby improving its cracking strength. On the other hand, the presence of longer fibers improves their adherence to the matrix, providing greater deformability to the material, which explains the reduction in the residual strengths.

6. CONCLUSIONS

This research explored the impact of the length and amount of steel fibers in the UHPFRC matrix to assess its effect. Once the most effective dosage and length were determined,

hybridization was carried out to determine whether it can help maintain or improve mechanical properties by reducing the total amount of steel used. The following conclusions were drawn from this research:

- Microscopic analysis shows that 13 mm steel fibers achieve better alignment and distribution within the UHPFRC matrix, resulting in an optimized bridging effect across cracks compared to 6 mm fibers. This enhanced alignment contributes to improved mechanical properties, especially in flexural strengths.
- Porosimetry analysis indicates that the mix with 196 kg/m³ of 13 mm fibers has the lowest macroporosity, which positively correlates with higher compressive strength. The improved pore distribution in this dosage appears critical in reducing structural weakness.
- The workability tests revealed a linear trend where increasing fiber dosage decreased slump flow, indicating lower workability. However, all mixes maintain the parameters of self-compaction, and did not directly impact mechanical performance, allowing for higher fiber dosages without compromising strength.
- Across all compositions, 13 mm fibers consistently provided superior compressive and flexural properties compared to 6 mm fibers, making them more effective at enhancing UHPFRC's mechanical performance. The optimal dosage for compressive strength was 196 kg/m³ of 13 mm fibers, achieving the highest compressive resistance, while the flexural strength peaked at 226 kg/m³. These findings guided the choice of 196 kg/m³ as the baseline for hybridization.
- Among the hybridization mixes the 80/20 mix exhibited the highest flexural strength among all tested compositions reaching 25% LOP than F13_196, even surpasses the performance of a higher fiber dosage of 226 kg/m³. This hybrid mix maintained compressive strength stable to the 13 mm-only mix at 196 kg/m³, demonstrating that hybrid fiber combinations can optimize flexural performance in UHPFRC applications without compromising compressive strength, therefore proves to be the best in terms of flexural strength and cost effectiveness.

Acknowledgments

This research was funded by the Ministerio de Ciencia e Innovación of Spain under project number PID2019-110928RB-C33 and PID2023-147971OB-C32.

References

[1] Z. Fang, L. Hu, H. Jiang, S. Fang, G. Zhao, Y. Ma, Shear performance of high-strength friction-grip bolted shear connector in prefabricated steel–UHPC composite beams: Finite element modelling and parametric study, Case Stud Constr Mater 18 (2023) e01860. https://doi.org/10.1016/J.CSCM.2023.E01860.

[2] X. Shao, L. Deng, J. Cao, Innovative steel-UHPC composite bridge girders for long-span bridges, Front Struct Civ Eng 13 (2019) 981–989. https://doi.org/10.1007/s11709-019-0531-9.

[3] B. MacDougall, H. Hajiloo, S. Sarhat, J. Kabanda, M. Green, The Compressive Strength of Ultra-high Performance Concrete at Elevated Temperatures, in: R. Gupta, M. Sun, S. Brzev, M.S. Alam, K.T.W. Ng, J. Li, A. El Damatty, C. Lim (Eds.), Proceedings of the Canadian Society of Civil Engineering Annual Conference 2022, Springer Nature Switzerland, Cham, 2024: pp. 895–906. https://doi.org/https://doi.org/10.1007/978-3-031-35471-7_63.

[4] F. de Larrard, T. Sedran, Optimization of ultra-high-performance concrete by the use of a packing model, Cem Concr Res 24 (1994) 997–1009. https://doi.org/10.1016/0008-8846(94)90022-1.

[5] P. Richard, M. Cheyrezy, Composition of reactive powder concretes, Cem Concr Res 25 (1995) 1501–1511. https://doi.org/10.1016/0008-8846(95)00144-2.

[6] S. Abbas, A.M. Soliman, M.L. Nehdi, Exploring mechanical and durability properties of ultra-high performance concrete incorporating various steel fiber lengths and dosages, Constr Build Mater 75 (2015) 429–441. https://doi.org/10.1016/J.CONBUILDMAT.2014.11.017.

[7] J.D.R. Martínez, J.D. Ríos, H. Cifuentes, C. Leiva, Multi-Scale Toughening of UHPC: Synergistic Effects of Carbon Microfibers and Nanotubes, Fibers 13 (2025). https://doi.org/10.3390/fib13040049.

[8] D. Wang, C. Shi, Z. Wu, J. Xiao, Z. Huang, Z. Fang, A review on ultra high performance concrete: Part II. Hydration, microstructure and properties, Constr Build Mater 96 (2015) 368–377. https://doi.org/10.1016/J.CONBUILDMAT.2015.08.095.

[9] Y. Niu, J. Wei, C. Jiao, Crack propagation behavior of ultra-high-performance concrete (UHPC) reinforced with hybrid steel fibers under flexural loading, Constr Build Mater 294 (2021) 123510. https://doi.org/10.1016/J.CONBUILDMAT.2021.123510.

[10] Y. Aydın, C. Cakiroglu, G. Bekdaş, Z.W. Geem, Explainable Ensemble Learning and Multilayer Perceptron Modeling for Compressive Strength Prediction of Ultra-High-Performance Concrete, Biomimetics 9 (2024). https://doi.org/10.3390/biomimetics9090544.

[11] M. Amran, S.S. Huang, A.M. Onaizi, N. Makul, H.S. Abdelgader, T. Ozbakkaloglu, Recent trends in ultra-high performance concrete (UHPC): Current status, challenges, and future prospects, Constr Build Mater 352 (2022) 129029. https://doi.org/10.1016/J.CONBUILDMAT.2022.129029.

[12] S. Abbas, M.L. Nehdi, M.A. Saleem, Ultra-High Performance Concrete: Mechanical Performance, Durability, Sustainability and Implementation Challenges, Int J Concr Struct Mater 10 (2016) 271–295. https://doi.org/10.1007/s40069-016-0157-4.

[13] M. Skazlić, D. Bjegović, Toughness testing of ultra high performance fibre reinforced concrete, Mater Struct 42 (2009) 1025–1038. https://doi.org/10.1617/s11527-008-9441-3.

[14] H. Huang, X. Gao, K.H. Khayat, Contribution of fiber alignment on flexural properties of UHPC and prediction using the Composite Theory, Cem Concr Compos 118 (2021) 103971. https://doi.org/10.1016/J.CEMCONCOMP.2021.103971.

[15] J.P. Hwang, M. Kim, K.Y. Ann, Porosity generation arising from steel fibre in concrete, Constr Build Mater 94 (2015) 433–436. https://doi.org/10.1016/J.CONBUILDMAT.2015.07.044.

[16] C. Jiang, K. Fan, F. Wu, D. Chen, Experimental study on the mechanical properties and microstructure of chopped basalt fibre reinforced concrete, Mater Des 58 (2014) 187–193. https://doi.org/10.1016/J.MATDES.2014.01.056.

[17] E. Poveda, G. Ruiz, H. Cifuentes, R.C. Yu, X. Zhang, Influence of the fiber content on the compressive low-cycle fatigue behavior of self-compacting SFRC, Int J Fatigue 101 (2017) 9–17. https://doi.org/10.1016/J.IJFATIGUE.2017.04.005.

[18] J.D. Ríos, C. Leiva, M.P. Ariza, S. Seitl, H. Cifuentes, Analysis of the tensile fracture properties of ultra-high-strength fiber-reinforced concrete with different types of steel fibers by X-ray tomography, Mater Des 165 (2019) 107582. https://doi.org/10.1016/J.MATDES.2019.107582.

[19] J.D. Ríos, H. Cifuentes, C. Leiva, S. Seitl, Analysis of the mechanical and fracture behavior of heated ultra-high-performance fiber-reinforced concrete by X-ray computed tomography, Cem Concr Res 119 (2019) 77–88. https://doi.org/https://doi.org/10.1016/j.cemconres.2019.02.015.

[20] H. Huang, X. Gao, K.H. Khayat, A. Su, Influence of fiber alignment and length on flexural properties of UHPC, Constr Build Mater 290 (2021) 122863. https://doi.org/10.1016/J.CONBUILDMAT.2021.122863.

[21] H. Huang, X. Gao, L. Li, H. Wang, Improvement effect of steel fiber orientation control on mechanical performance of UHPC, Constr Build Mater 188 (2018) 709–721. https://doi.org/https://doi.org/10.1016/j.conbuildmat.2018.08.146.

[22] Z. Wu, C. Shi, W. He, D. Wang, Static and dynamic compressive properties of ultra-high performance concrete (UHPC) with hybrid steel fiber reinforcements, Cem Concr Compos 79 (2017) 148–157. https://doi.org/10.1016/J.CEMCONCOMP.2017.02.010.

[23] D.J. Kim, S.H. Park, G.S. Ryu, K.T. Koh, Comparative flexural behavior of Hybrid Ultra High Performance Fiber Reinforced Concrete with different macro fibers, Constr Build Mater 25 (2011) 4144–4155. https://doi.org/10.1016/J.CONBUILDMAT.2011.04.051.

[24] B. Chun, D.Y. Yoo, Hybrid effect of macro and micro steel fibers on the pullout and tensile behaviors of ultra-high-performance concrete, Compos B Eng 162 (2019) 344–360. https://doi.org/10.1016/J.COMPOSITESB.2018.11.026.

[25] D.Y. Yoo, S.W. Kim, J.J. Park, Comparative flexural behavior of ultra-high-performance concrete reinforced with hybrid straight steel fibers, Constr Build Mater 132 (2017) 219–229. https://doi.org/10.1016/J.CONBUILDMAT.2016.11.104.

[26] W. Chen, Y. Wen, Experimental study on mechanical and durability properties of concrete incorporating various polyvinyl alcohol fiber lengths and dosages, Mater Construcc74 (2024) e349. https://doi.org/10.3989/mc.2024.368923.

[27] European Committee for Standarization (CEN), EN 197-1: Cement - Part 1: Composition, specifications and conformity criteria for common cements, Brussels, Belgium, 2011.

[28] D.Y. Yoo, J.H. Lee, Y.S. Yoon, Effect of fiber content on mechanical and fracture properties of ultra high performance fiber reinforced cementitious composites, Compos Struct 106 (2013) 742–753. https://doi.org/10.1016/J.COMPSTRUCT.2013.07.033.

[29] J.D. Ruiz Martínez, J.D. Ríos, E.M. Pérez-Soriano, H. Cifuentes, C. Leiva, Enhancing the matrix-fiber bond in ultra-high-performance fiber-reinforced concrete using a high performance plasticizer. Impact on the flowability, physical and mechanical properties, Constr Build Mater 470 (2025) 140683. https://doi.org/10.1016/J.CONBUILDMAT.2025.140683.

[30] European Committee for Standardization (CEN), EN 12350-2: Testing fresh concrete - Part 2: Slump test., Brussels, Belgium, 2020.

[31] E. Nguyen Amanjean, M. Mouret, T. Vidal, Effect of design parameters on the properties of ultra-high performance fibre-reinforced concrete in the fresh state, Constr Build Mater 224 (2019) 1007–1017. https://doi.org/10.1016/J.CONBUILDMAT.2019.07.284.

[32] T. Park, S. Her, H. Jee, S. Yoon, B. Cho, S.H. Hwang, S. Bae, Evaluation of orientation and distribution of steel fibers in high-performance concrete column determined via micro-computed tomography, Constr Build Mater 270 (2021) 121473. https://doi.org/10.1016/J.CONBUILDMAT.2020.121473.

[33] J. Zhou, J. Lai, L. Du, K. Wu, S. Dong, Effect of directionally distributed steel fiber on static and dynamic properties of 3D printed cementitious composite, Constr Build Mater 318 (2022) 125948. https://doi.org/10.1016/J.CONBUILDMAT.2021.125948.

[34] J. Liu, M. An, L. Huang, Y. Wang, S. Han, Influence of vibrating compaction time on the strength and microstructure of ultra-high performance concrete, Constr Build Mater 409 (2023) 133584. https://doi.org/10.1016/J.CONBUILDMAT.2023.133584.

[35] European Committee for Standardization (CEN), EN- 12390-3: Testing hardened concrete - Part 3: Compressive strength of test specimens, Brussels, Belgium, 2020.

[36] European Committee for Standardization (CEN), EN 14651: Test method for metallic fibre concrete - Measuring the flexural tensile strength (limit of proportionality (LOP), residual), Brussels, Belgium, 2008.

[37] H. Abdolpour, P. Niewiadomski, Ł. Sadowski, A. Chowaniec, Self-compacting ultra-high performance mortars produced with waste catalysts from petrochemical industry: Rheological, mechanical and microstructural properties, J Clean Prod 369 (2022) 133225. https://doi.org/10.1016/j.jclepro.2022.133225.

[38] S.T. Kang, J.K. Kim, The relation between fiber orientation and tensile behavior in an Ultra High Performance Fiber Reinforced Cementitious Composites (UHPFRCC), Cem Concr Res 41 (2011) 1001–1014. https://doi.org/10.1016/J.CEMCONRES.2011.05.009.

[39] R. Mu, J. Chen, X. Chen, C. Diao, X. Wang, L. Qing, Effect of the orientation of steel fiber on the strength of ultra-high-performance concrete (UHPC), Constr Build Mater 406 (2023) 133431. https://doi.org/10.1016/J.CONBUILDMAT.2023.133431.

[40] J.D. Ruiz Martínez, J.D. Ríos, E.M. Pérez-Soriano, H. Cifuentes, C. Leiva, Effect of nano silicon nitride on the microstructural characteristics and mechanical properties of ultra-high-performance steel fiber reinforced concrete, Mater Struct 58 (2025) 103. https://doi.org/10.1617/s11527-025-02634-9.

[41] S.P. Shah, Determination of fracture parameters (K Ic s and CTOD c) of plain concrete using three-point bend tests, Mater Struct 23 (1990) 457–460. https://doi.org/https://doi.org/10.1007/BF02472029.

[42] Z.P. Bažant, M.T. Kazemi, Determination of fracture energy, process zone longth and brittleness number from size effect, with application to rock and conerete, Int J Fract 44 (1990) 111–131. https://doi.org/https://doi.org/10.1007/BF00047063.

[43] Z.P. Bažant, E. Becq-Giraudon, Statistical prediction of fracture parameters of concrete and implications for choice of testing standard, Cem Concr Res 32 (2002) 529–556. https://doi.org/10.1016/S0008-8846(01)00723-2.

[44] W. Meng, K.H. Khayat, Mechanical properties of ultra-high-performance concrete enhanced with graphite nanoplatelets and carbon nanofibers, Compos B Eng 107 (2016) 113–122. https://doi.org/10.1016/J.COMPOSITESB.2016.09.069.

[45] V. Ortega-López, A. García-Llona, V. Revilla-Cuesta, A. Santamaría, J.T. San-José, Fiber-reinforcement and its effects on the mechanical properties of high-workability concretes manufactured with slag as aggregate and binder, J Build Eng 43 (2021) 102548. https://doi.org/10.1016/J.JOBE.2021.102548.

[46] H. Zhang, B. He, X. Zhu, Q. Wang, Z. Jiang, The use of AE technique for identifying ductility degradation against cryogenic on flexural performance of UHPC at various temperature conditions, Cem Concr Compos 137 (2023) 104904. https://doi.org/10.1016/J.CEMCONCOMP.2022.104904.

[47] Y. Wang, S. Backer, V.C. Li, An experimental study of synthetic fibre reinforced cementitious composites, J Mater Sci 22 (1987) 4281–4291. https://doi.org/10.1007/BF01132019.

[48] J.D. Ríos, C. Leiva, A. de la Concha, M.P. Ariza, H. Cifuentes, Influence of Graphene Oxide Concentration and Ultrasonication Energy on Fracture Behavior of Nano-Reinforced Cement Pastes, Crystals (Basel) 14 (2024). https://doi.org/10.3390/cryst14080707.

[49] A. Martínez-de-la-Concha, J.D. Ríos, H. Cifuentes, Numerical Study of the Shear Behavior of Ultra-High-Performance Concrete Beams, Hormigón Acero 75 (2024) 157–162.